Available online at www.sciencedirect.com
SCIENCE DIRECT®
Journal of Nuclear Materials 350 (2006) 74–82
journal of nuclear materials
www.elsevier.com/locate/jnucmat

The influence of roughness on tribological properties of nuclear grade graphite

Luo Xiaowei *, Yu Suyuan, Sheng Xuanyu, He Shuyan

INET, Tsinghua University, Beijing 100084, China

Received 17 January 2005; accepted 22 November 2005

Abstract

The influence of surface roughness on tribological properties of graphite IG-11 was investigated on a standard SRV tester. The experimental condition was selected as: 30 N normal load, room temperature and a 10 Hz frequency with different strokes. The experiments environments included helium and air. Five types of roughness were studied in the experiments. The experiments revealed that the surface roughness greatly affected the graphite friction behavior. When the friction surface was smooth, the friction coefficient was high because of intensive adhesion accompanied by many pits at the friction surface. When the friction surface was rough, the adhesion was very poor, but the wear was excessive and generated many graphite particles at the friction surface. These particles can separate the friction surfaces, which reduced the friction action between them. For very rough specimens, the friction coefficient decreased with sliding velocity at about 0.004 m/s and then increases gradually.

PACS: 28.41.Qb

1. Introduction

Graphite is widely used in reactors, especially in Gas-cooled Reactors (GCR) because of its excellent nuclear properties (graphite is an excellent solid moderator and has good irradiation performance), high thermal conductivity, good mechanical properties at high temperatures, good machining characteristics, good corrosion resistance and a mature manufacturing process. Graphite IG-11 was used in 10 MW High Temperature Gas-cooled Reactor (HTR-10) as the moderating material and structure material. In the HTR-10, there are about 60 tons graphite IG-11 used as the moderating material. Graphite IG-11 has been the focus of many researches, mainly on its irradiation effect and mechanical analysis. However, studies on the tribological properties of graphite IG-11 are rare. HTR-10 is a pebble bed reactor, and each fuel ball will pass through the reactor core several times. The movements of the fuel ball, the temperature and irradiation inhomogeneities, and other impact loads make friction and wear inevitable in HTR-10. Moreover, the design of the lifting velocity of fuel elements in charge tube also needs to know the tribological properties of graphite. Authors have made

* Corresponding author. Tel.: +86 10 6278 4824; fax: +86 10 6277 1150.
E-mail address: xwluo@tsinghua.edu.cn (L. Xiaowei).

0022-3115/$ - see front matter © 2005 Elsevier B.V. All rights reserved.
doi:10.1016/j.jnucmat.2005.11.013

Nomenclature

a	radius of contact area of a deformed asperity
A_n	nominal contact area
d	separation based on the asperity heights
E	$\left(\frac{1-v_1^2}{E_1}+\frac{1-v_2^2}{E_2}\right)^{-1}$, equivalent elastic modulus
E_1, E_2	elastic moduli of the contacting materials
F	applied load
F_s	adhesion force
F_s^*	dimensionless adhesion force, F_s/A_nE
G	$\frac{2-v_1}{G_1}+\frac{2-v_2}{G_2}$
G_1, G_2	shear moduli of the contacting materials, $\frac{E_1}{2(1+v_1)}$ or $\frac{E_2}{2(1+v_2)}$
H	hardness of graphite
h	separation based on the surface heights
h^*	dimensionless mean separation, h/σ_e
K	hardness coefficient
P	total contact load
P^*	dimensionless contact load, $P/(A_nE)$
Q	the tangential force
r	radial coordinate of asperity contact region
R_1, R_2	asperity radius of curvature of contacting surfaces
R_e	asperity radius of curvature for equivalent rough surface, $R_1 \cdot R_2/(R_1+R_2)$
s	$(r^2-a^2)^{1/2}$
s^*	$s/\sqrt{R_e\sigma_e}$
y_s	distance between the mean of asperity heights and that of surface heights
y_s^*	y_s/σ_e
z	height of asperity measured from the mean of asperity heights
z^*	dimensionless height of asperity, z/σ_e
Z	separation of the contacting sphere and the plat outside the contact area
Z^*	Z/σ_e
β	$\eta R_e\sigma_e$
γ	work of adhesion per unit area
ε	intermolecular distance (0.3–0.5 nm)
ε^*	ε/σ_e
η	areal density of asperities
λ	plastic adhesion index
μ_a	adhesion component in friction coefficient
v	Poisson's ratio
θ	elastic adhesion index
σ_e	$(\sigma_1^2+\sigma_2^2)^{1/2}$, equivalent standard deviation of the asperity heights
σ_1, σ_2	surface heights standard deviation of the contacting surfaces
σ_s	equivalent standard deviation of the surface heights
ϕ	distribution function of asperity heights
ϕ^*	dimensionless distribution function
w	interference
w^*	dimensionless interference, w/σ_e
w_c	critical interference at the inception of plastic deformation
w_c^*	dimensionless critical interference, w_c/σ_e

some research about tribological properties of graphite IG-11 [1–4]. The present work is to investigate the influence of surface roughness on the tribological properties. Graphite IG-11 is manufactured by the Toyo Tanso Co. Ltd., Japan. The main parameters of IG-11 are shown in Table 1 [1].

2. Apparatus and specimens

The apparatus was a standard SRV tester, a high temperature wear and friction apparatus, from the Optimol Company, Germany. The temperature could be continuously adjusted between −40 °C and 900 °C. The normal load, stroke and frequency could also continuously be adjusted and the experimental environment could be controlled. Experi-

Table 1
The main parameters of graphite IG-11

Granularity (mm)	0.02
Density (g/cm^3)	1.76
Dynamic elastic modulus (GPa)	9.04
Compression strength (MPa)	68.65
Fracture toughness (MPa m$^{1/2}$)	0.945
Possion's ratio	0.126
Tensile strength (MPa)	23.05
Thermal conductivity (W/m/°C)	144
Thermal expansion coefficient (10^{-6}/°C)	3.9
Brinell hardness	17

Note: dynamic elastic modulus, compression strength, fracture toughness, thermal conductivity, thermal expansion coefficient, tensile strength and Brinell hardness in Table 1 were all measured in the perpendicular direction to crystal tendency.

mental conditions were chosen to investigate the influence of surface roughness. The normal load was set as 30 N related to static pressure from the gravity of graphite block in reactor core, and the experiments were conducted at room temperature. The influence of temperature on tribological behavior of IG-11 can see in [4]. The influence of pressure was not our concern in this paper, and the experimental pressure was selected as one atmospheric pressure. The experimental frequency was 10 Hz with strokes of 0.01 mm, 0.1 mm, 0.2 mm, 0.4 mm, 0.8 mm and 2 mm. The specimens were machined from a graphite block that was used in HTR-10. The dimensions of the specimens are shown in Fig. 1. In the experiments, five types of surface roughness were machined to study the influence of surface roughness. Talysurf 5-120 was used to measure the initial surface roughness of the specimens. Different profiles of friction surfaces are shown in Fig. 2. 3200 digital points were sampled in the radial direction of specimens. The spacing of the digital points was 1.25 μm. The total sampling length was 4 mm. Roughness parameters for specimens with different roughness are listed in Table 2.

3. Experimental results

Fig. 3 shows the variation friction coefficient with sliding velocity for each type of roughness specimen at a given experimental condition (in air). The results revealed an obvious influence of surface roughness on the friction coefficient. The friction coefficient had an increasing trend corresponding to the surface roughness. For example, when the sliding velocity was 0.08 m/s, the friction coefficients were 0.29, 0.26, 0.24, 0.21 and 0.20, respectively, corresponding to specimens #1, #2, #3, #4 and #5. Furthermore, if the surface roughness exceeded a certain value, the friction coefficients decreased with sliding velocity at about 0.004 m/s and reached a minimum value at about 0.016 m/s. Then the friction coefficients increased with sliding velocity again.

The experimental results for specimens in helium are shown in Fig. 4. The friction coefficient also decreased with surface roughness as the experiments in air. When the sliding velocity was 0.08 m/s, the friction coefficient of specimen #5 was 0.2, and the friction coefficient of #2 was 0.41, over two times that of #5. At the same sliding velocity, in helium, the friction coefficient of graphite specimens for the same roughness was larger than that in air.

4. Analysis of friction surfaces

A scanning electron microscope (SEM) was applied to analyze the friction surfaces. Fig. 5 shows the friction surfaces of lower specimens in air with different roughnesses. The friction surfaces were magnified 500 times. For different roughnesses, the friction surfaces exhibited different characteristics. Fig. 5(a) is an enlarged view of specimen #1. It is clearly shown that severe adhesion occurred at the friction surface. There were many pits caused by adhesion tearing. The friction surface was very clean and did not have any abrasive dust. Fig. 5(b) is a magnified view of specimen #2, and the surface characteristics are visibly different from specimen #1. On the friction surface, there was a little abrasive dust. There was also a large granule and some

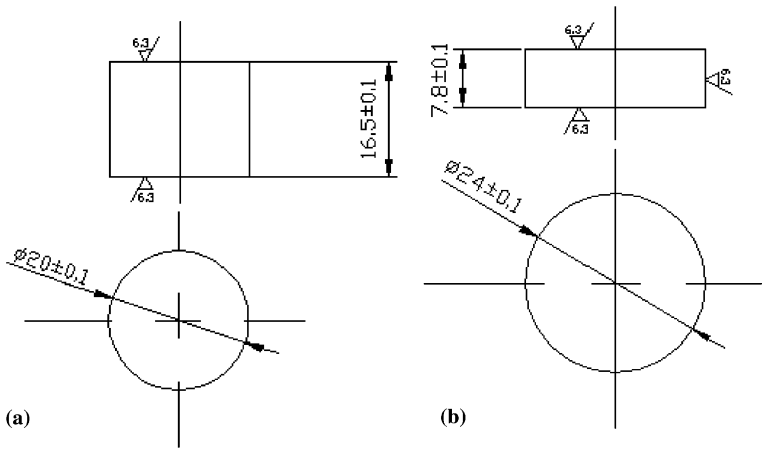

Fig. 1. The dimensions of the specimens. (a) Upper specimens; (b) lower specimens.

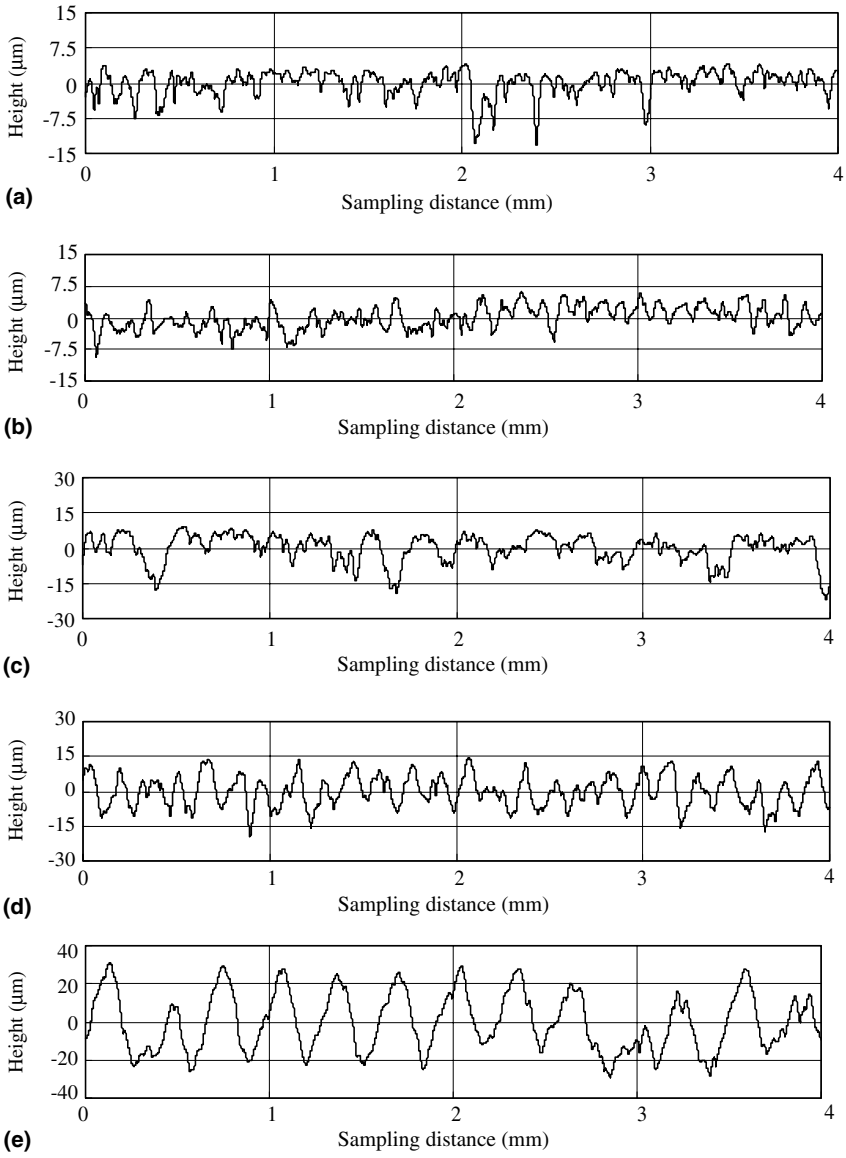

Fig. 2. The topography analysis of specimen surfaces. (a) Specimen #1; (b) Specimen #2; (c) Specimen #3; (d) Specimen #4; (e) Specimen #5.

Table 2
The original roughness parameters of specimens of different roughnesses

Specimen type	R_a, Arithmetical mean deviation of surface height (μm)	σ, Standard deviation of surface heights (μm)	S, Mean spacing of asperity (μm)	R^{-1}, Mean of asperity curvature (1/μm)
#1	2.04	2.66	23.82	0.0343
#2	2.23	2.86	22.67	0.0495
#3	4.62	5.72	24.25	0.0509
#4	5.59	6.66	34.19	0.0550
#5	13.39	15.49	50.83	0.0636

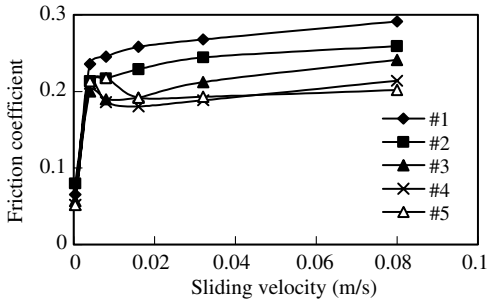

Fig. 3. The friction coefficient for specimens with different roughnesses (in air).

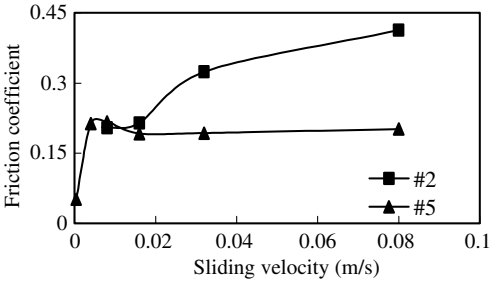

Fig. 4. The friction coefficient for specimens with different roughness (in helium).

dusts adhering to the friction surface as a result of a jostling action between friction surfaces. The friction surfaces of specimens #3 and #4 are shown in Fig. 5(c) and (d). There were many thin particles at the friction surface. These particles adhered to the friction surface by Van der Waals force and can be migrated during the course of friction due to the action of friction force. The friction surface of specimen #5 with a fairly rough surface is shown in Fig. 5(e). Specimen #5 contained region in which friction occurred. There was still a large area that did not rub. In the contact region, there were also many thin abrasive particles. The friction surfaces in helium were similar to those in air. When the friction surface was smooth, adhesion took place at the friction surface. When the friction surface was rough, the friction surfaces had many abrasive particles.

5. Discussion

For graphite IG-11 specimens with different surface roughnesses, the tribological properties exhibited in the experiments were not the same. The friction coefficient of graphite specimens with smooth surfaces was higher than that of specimens with rough friction surfaces. This difference mainly arises from the difference in the real contact area between friction surfaces and the loading mode (elastic or plastic loading) of asperities during the friction course. The adhesion forces between the upper and the lower friction surfaces vary with surface roughness, and these further change the value of the friction coefficient. Greenwood and Tripp [5] pointed out that the contacts of two rough surfaces can be modeled by an equivalent single surface contacting a rigid smooth plane. The equivalent rough surface defined as the one whose asperity curvature is the sum of the two curvatures and whose height distribution is that of the sum of the height of the original pair. Many researches have been conducted on the adhesion and contact, and two famous physical models have been formed: Johnson–Kendall–Roberts model (JKL model) [6] and Derjaguin–Muller–Toporov model (DMT model) [7]. JKR argued that the attractive surface force increased the contact area beyond that predicted by the Hertz equation [8]. But DMT thought the contact area, predicted by the Hertz equation, was unaffected by the attractive surface force and the surface force were exerted outside the contact area. Muller et al. [9] pointed out two models are the limiting cases of a general solution. They introduced a parameter to select a model suitable for application. The DMT model holds for harder materials with high elastic modulus. The JKR model is suitable for the soft material with low elastic modulus. Chowdhury and Ghosh [10] studied the adhesion and adhesional friction between two solids using the JKR model. They introduced two adhesion index θ (elastic adhesion index) and λ (plastic adhesion index) to describe adhesion and adhesional friction. On the basis of Greenwood and Wiliamson's [11] rough surface model, the formula to calculate the loading force and unloading force were developed. They found the adhesion was strong at the low value of elastic adhesion index θ and it was very little affected by the change in λ. The adhesion index's θ and λ were defined as follows:

$$\theta = \frac{E\sigma_e^{3/2}R_e^{1/2}}{R_e\gamma}, \quad \lambda = \frac{\pi^2 R_e H^4 \sigma_e}{18E^2\gamma^2},$$

where E is the equivalent Young's modulus of two materials; R_e is the equivalent radius of curvature of asperity; σ_e is the equivalent asperity heights standard deviation of two rough surfaces; H is the

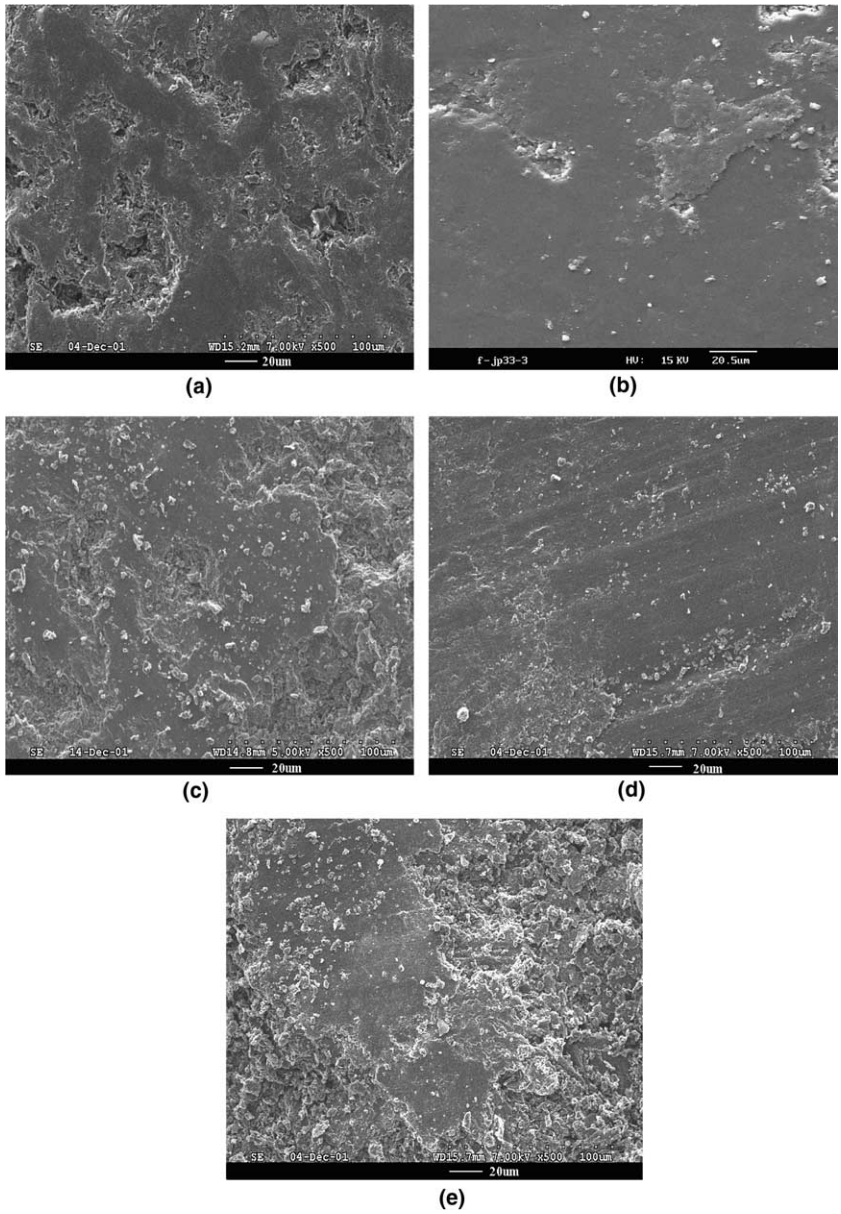

Fig. 5. The SEM analysis of friction surfaces (in air). (a) #1; (b) #2; (c) #3; (d) #4; (e) #5.

hardness of surface; γ is work of adhesion per unit area and equals $\gamma_1 + \gamma_2 - \gamma_{12}$; γ_1 and γ_2 are the surface energy of contacting surfaces, γ_{12} is the surface energy of contacting interface.

Chang et al. [12] analyzed the adhesion between metallic rough surfaces using the DMT model. They also found the adhesion force was strong at a low value of adhesion index θ. Since the elastic modulus of graphite is very high, we can use the result of Chang et al. [12]. The adhesion force can be calculated by the following formula:

$$F_s^*(h^*) = \frac{8\pi\eta R_e}{3E}\gamma\varepsilon^{*2}\left\{\int_{-\infty}^{h^*-y_s^*}\left[\left(\frac{1}{\varepsilon^*-w^*}\right)^2 - 0.25\frac{\varepsilon^{*6}}{(\varepsilon^*-w^*)^8}\right]\times\phi^*(z^*)\,\mathrm{d}z^* + 2\int_{h^*-y_s^*}^{\infty}\int_0^{\infty}\left(\frac{1}{Z^{*3}}-\frac{\varepsilon^{*6}}{Z^{*9}}\right)\phi^*(z^*)s^*\,\mathrm{d}s^*\,\mathrm{d}z^*\right\} \quad (1)$$

where F_s^* is the dimensionless adhesion force, $F_s/(A_nE)$; F_s, A_n and E are the adhesion force, nominal contact area and equivalent elastic modulus, respectively. h^* is the dimensionless mean separation, h/σ_s; h is the separation based on the surface heights and

σ_s is the standard deviation of surface height for the equivalent rough surface. $\phi^*(z^*)$ is the normalized distribution function of the asperity heights. For a Gaussian distribution of asperity heights, $\phi^*(z^*)$ is

$$\phi^*(z^*) = (2\pi)^{-1/2}\left(\frac{\sigma_s}{\sigma_e}\right)\exp\left[-0.5\left(\frac{\sigma_s}{\sigma_e}\right)^2 z^{*2}\right]. \quad (2)$$

z^* is the dimensionless height of asperity, z/σ_s, and z is the height of asperity measured from the mean of asperity heights. η is the areal density of asperities. ε^* equals ε/σ_s, ε is the intermolecular distance (0.3–0.5 nm). y_s^* equals y_s/σ_s and y_s is the distance between the mean of asperity heights and that of surface heights. w^* is the dimensionless interference, w/σ, and $w^* = z^* - h^* + y_s^*$, w is the interference. Z^* equals Z/σ_s, and Z is the separation of the contacting sphere and the plate outside the contact area. For elastic contact between a sphere and a plate, the profile outside the contact area can be obtained from the Hertz solution. It was presented by Muller et al. [13] in the form

$$Z(r,a) = \frac{1}{\pi R_e}\left[a(r^2-a^2)^{1/2} - (2a^2-r^2)\tan^{-1}\left(\frac{r^2}{a^2}-1\right)^{1/2}\right] + \varepsilon, \quad (3)$$

where r is the radial coordinate of asperity contact region, and a is the radius of contact area of a deformed asperity, $(wR_e)^{1/2}$. s^* equals s/σ_s, and $s = (r^2-a^2)^{1/2}$.

The dimensionless contact load was given by Chang et al. [14] as:

$$P^*(h^*) = \beta\left\{\frac{4}{3}(\sigma_s/R_e)^{1/2}\int_{h^*-y_s^*}^{h^*-y_s^*+w_c^*} w^{*3/2}\phi^*(z^*)\,dz^* + \pi K\frac{H}{E}\int_{h^*-y_s^*+w_c^*}^{\infty}(2w^*-w_c^*)\phi^*(z^*)\,dz^*\right\} \quad (4)$$

where P^* is the dimensionless contact load, $P/(A_nE)$, and P is the contact load. $\beta = \eta R_e\sigma$, w_c^* is the dimensionless critical interference, w_c/σ_s, and w_c is the critical interference at the inception of plastic deformation. K is a hardness coefficient related to the Poisson ratio, v. The values of w_c and K were given by Chang [15]

$$w_c = \left(\frac{\pi KH}{2E}\right)^2 R_e, \quad K = 0.454 + 0.41v. \quad (5)$$

In reference to [16], McCool gave the relation between h and σ_s for the surface microgeometry model and d (separation based on asperity heights) and σ_e for the asperity-based model. At the same time, a formula was given to calculate the value of y_s

$$\sigma_s^2 = \sigma_e^2 + \frac{3.717\times10^{-4}}{\eta^2 R_e^2}, \quad (6)$$

$$h = d + y_s, \quad (7)$$

$$y_s = 4\left(\frac{m_0}{\pi\alpha}\right)^{1/2}, \quad (8)$$

where

$$\alpha = \frac{m_0 m_4}{m_2^2} \quad (9)$$

and m_0, m_2 and m_4 are defined for a surface profile $y(x)$ as

$$m_0 = \mathrm{AVG}[y^2], \quad (10)$$

$$m_2 = \mathrm{AVG}\left[\left(\frac{dy}{dx}\right)^2\right], \quad (11)$$

$$m_4 = \mathrm{AVG}\left[\left(\frac{d^2y}{dx^2}\right)^2\right]. \quad (12)$$

Using the above formulas and the surface topography data, we can get the values of y_s and σ_s (listed in Table 3). In this experiment, the experimental applied load was 30 N, which equals to the contact load subtracting the adhesion force. The equivalent elastic modulus of graphite was 4.593×10^9 Pa. The areal densities of asperity η for different specimens are given in Table 3. Literature [17] gave the surface energy of anisotropic graphite. The basal face energy was 0.1–0.2 J/m^2, and the prismatic face energy was 5 J/m^2 (in vacuum). For near isotropic graphite IG-11, we selected $\gamma = 2.6$ J/m^2, the mean value of basal face and prismatic face since the graphite is a polycrystal. Employing $\varepsilon = 0.4$ nm and combining Eqs. (1) and (4), we obtained the dimensionless separation of two surfaces during loading, the adhesion force and contact load (listed in Table 3). The relationship of the adhesion force for the five specimens is: #1 > #2 > #3 > #4 > #5. The adhesion force of #1 is 4.35 times as large as the force of #5.

Savkoor and Briggs [18] obtained the relationship for applied load, adhesion force and tangential force through analysis of the energy balance. They found that as the tangential force T increased, the area of contact reduced in a stable manner until a critical value T_0. When the tangential force exceeded

Table 3
The values of main parameters used in calculation of adhesion force

Specimen type	y_s (μm)	σ_s (μm)	η (m^{-2})	h^*	$F_s(N)$	$P(N)$	μ_a
#1	1.405	3.686	1.762×10^9	2.7054	15.47	45.46	0.366
#2	1.271	3.924	1.946×10^9	2.5666	14.29	44.30	0.342
#3	2.389	8.007	1.701×10^9	2.8201	7.92	37.92	0.210
#4	3.343	9.087	8.555×10^9	2.6238	6.82	36.82	0.186
#5	3.514	20.097	3.870×10^9	2.4096	3.56	33.57	0.111

the critical value T_0, the reduction in area became unstable and separation may occur. The critical tangential force is given by

$$T_0 = \frac{2}{(EG)^{1/2}}(6\gamma\pi R_e P_0 + 9\gamma^2\pi^2 R_e^2)^{1/2}, \tag{13}$$

where

$$G = \frac{2-v_1}{G_1} + \frac{2-v_2}{G_2}.$$

P_0 is applied load. Consider the DMT model, for the elastic contact, $P_0 = \frac{4}{3}ER_e w^{3/2}$; for the plastic contact, $P_0 = \pi R_e w(2-\frac{w_c}{w})KH$. The total tangential force between contacting surfaces is

$$\begin{aligned} Q = \frac{2\eta A_n}{(EG)^{1/2}}\Bigg\{ & \int_d^{d+w_c} (8\gamma\pi E R_e^{3/2} w^{3/2} \\ & + 9\gamma^2\pi^2 R_e^2)^{1/2}\phi(z)\,dz \\ & + \int_{d+w_c}^{\infty} [6\gamma\pi^2 R_e^2 KH(2w - w_c) \\ & + 9\gamma^2\pi^2 R_e^2]^{1/2}\phi(z)\,dz \Bigg\} \end{aligned} \tag{14}$$

where Q is the tangential force due to adhesion between the contacting surfaces. The adhesion component in friction coefficient due to the adhesion between contacting surfaces is

$$\mu_a = \frac{Q}{P - F_s} = \frac{Q}{F}. \tag{15}$$

F is the applied load. From Eqs. (14) and (15), we can calculate the adhesion component in friction coefficient for each roughness specimen (listed in Table 3). The order of μ_a is: #1 > #2 > #3 > #4 > #5. The adhesion component in friction coefficient of specimen #1 is 0.366 and is 3.0 times as large as that of specimen #5. This reveals that the adhesion component in friction coefficient is dominating when the friction surface is smooth; on the contrary, the adhesion component is small for the rough friction surface. The value μ_a of #1 is greater than the friction coefficient of specimen #1 in air. The reason is that in air, the surface energy of graphite (calculation using the surface energy in vacuum) degrades due to the passivation by the chemical/physical adsorption so that the work of adhesion γ decrease, which results in a decrease in adhesion component in friction coefficient and induces the low coefficient in air. In helium, the passivation does not occur due to chemical inertia so that the graphite surfaces have high surface energy. As a result, the adhesion component in friction coefficient is larger in helium than in air. For specimen #5, the adhesion component in friction coefficient is much small comparing to the fiction coefficient in air. The reason is that the component in friction coefficient due to mechanical engagement increases with surface coarseness.

Furthermore, we noted that there was a lager amount of abrasive particles on the friction surfaces of very rough specimens, such as #3, #4 and #5. Under the same contact load, the rougher the contact surfaces are, the smaller the contact area is and the more intensive the stress of asperity is. Because the material is brittle, the brittle fracture failures will occur and generate abrasive particles when the stress is beyond the endurance range of graphite. These graphite particles cover the friction surfaces. With the action of normal force, the particles intimately jostled to the surface and adhered to it by Van der Waals force. But the particles can still move by the action of friction force. These abrasive particles formed so-called the third-body layer to separate the two friction surfaces [19]. The third-body layer acts as a soft, low shear stress solid lubricant to reduce the friction force. For very rough surfaces, the friction coefficient decreases as shown in Fig. 3. With further sliding, the abrasive particles move to the outsides of the contact surfaces by the action of the friction force. So the friction coefficient resumes a gradual increase.

For specimen #1, there are many pits at the friction surfaces. Under the action of the normal load and friction force, the maximum tensile region

originates at the back edge contact. The tensile region increases with the increase of friction force. For brittle material, crack and pits are formed when there is enough tensile strength. If the von Mises yielding criteria is used, the maximum equivalent stress region appears in the back edge of the contact when the friction is great enough [20,21].

6. Conclusion

The surface roughness can greatly affect graphite friction behaviors. When the friction surface is smooth, the friction coefficient is high because of the excessive adhesion between friction surfaces accompanied by many pits at the friction surfaces caused by intensive adhesion. When the friction surface is rough, the adhesion is very poor, but the wear is excessive and generates many particles. These particles can separate the friction surfaces to reduce the friction action between friction surfaces. For very rough specimens, the friction coefficient decreases at first and then increases gradually.

Acknowledgements

This publication was made possible by grant number 50006005 from the Natural Science Foundation of China, the Outstanding Young Professor Prize of the National Education Commission, Start-up Fund for Scholars Returning from Oversea and the Research Fund from the Environmental Institute of Tsinghua University. Authors appreciated above supports.

References

[1] X. Luo, S. Yu, X. Sheng, S. He, Math. Phys. Astron. 44 (2001) 248.
[2] X. Luo, S. Yu, X. Sheng, S. He, High Technol. Lett. 11 (2001) 97.
[3] X. Luo, S. Yu, X. Sheng, S. He, Atom. Energy Sci. Technol. 38 (2004) 226.
[4] X. Luo, S. Yu, X. Sheng, S. He, Tribology 24 (2004) 402.
[5] J.A. Greenwood, J.H. Tripp, Proc. Inst. Mech. Engrs. 185 (1971) 625.
[6] K.L. Johnson, K. Kendall, A.D. Roberts, Proc. R. Soc. Lond. A 324 (1971) 301.
[7] B.V. Derjaguin, V.M. Muller, Yu.P. Toporov, J. Colloid Interf. Sci. 53 (1975) 314.
[8] H. Hertz, J. Reine Angew. Math. 92 (1882) 156.
[9] V.M. Muller, V.S. Yushchenko, B.V. Derjaguin, J. Colloidal Interface Sci. 66 (1980) 991.
[10] S.K. Roy Chowdhury, P. Ghosh, Wear 174 (1994) 9.
[11] J.A. Greenwood, J.B.P. Williamson, Proc. R. Soc. Lond. A 295 (1966) 300.
[12] W.R. Chang, I. Etsion, D.B. Bogy, J. Tribol. 109 (1987) 257.
[13] V.M. Muller, B.V. Derjaguin, Y.P. Toporov, Colloids Surf. 7 (1983) 251.
[14] W.R. Chang, I. Etsion, D.B. Bogy, J. Tribol. 110 (1988) 50.
[15] W.R. Chang, PhD thesis, University of California, Berkeley, 1986.
[16] J.L. McCool, ASME J. Tribol. 108 (1986) 380.
[17] P.J. Bryant, P.L. Gutshall, L.H. Taylor, Mechanics of Solid Friction, Elsevier, Amsterdam, 1964.
[18] A.R. Savkoor, G.A.D. Briggs, Proc. R. Soc. Lond. A 356 (1977) 103.
[19] M. Godet, Wear 100 (1984) 437.
[20] G.M. Hamilton, Proc. Inst. Mech. Engrs. 197 (1983) 53.
[21] B. Bhushan, Appl. Mech. Rev. 49 (1996) 275.